48th AIAA Aerospace Sciences Meeting Including the New Horizons Forum and Aerospace Exposition
4 - 7 January 2010, Orlando, Florida

Linear Stability Analysis of Nose Bluntness Effects on Hypersonic Boundary Layer Transition

Jia Lei * and Xiaolin Zhong†
University of California, Los Angeles, California 90095

Transition reversal on blunt cone hypersonic boundary layer transition refers to the experimental observation that the laminar-turbulent transition location moves upstream with increasing nose radius when it is larger than a certain critical value. It was first reported in Stetson's transition experiment in 1967on a Mach 5.5 flow over blunt cones. Decades passed, the cause of reversal is still not well understood. In all previous linear stability and numerical simulation on different study cases, no bluntness-caused reversal was found. The objective of this paper is to perform extensive linear stability analysis on Stetson's Mach 5.5 cases. Three different blunt cones with nose radii of 0.156, 0.5 and 1.5 inch will be used to study the effect of nose bluntness on transition.

1. INTRODUCTION

For hypersonic flows over blunt cones, the transition location moves downstream when the nose radius increases. This trend is, however, reversed when the nose radius is larger than certain critical value based on some experimental observations [1, 20]. This phenomenon is called transition reversal. Increasing nose radius after that will lead to a forward movement of the transition location. The downstream movement of the transition location at small radii can be explained by the reduction of local Reynolds numbers owing to the entropy layer created by the nose bluntness. However, there is still no satisfactory explanation for the cause of transition reversal at large nose bluntness.

Most of the previous theoretical and computational studies of the transition reversal have been on the Stetson's stability experiments on an axisymmetric blunt cone in a Mach 7.99 flow [2, 3]. The half angle of the cone was 7^o, the nose radii were up to 1.5 inches and larger, and the freestream Reynolds number based on the nose radius was 33,449. The Reynolds number based on the total length of the cone was about 9 millions. Detailed fluctuation spectra of the disturbance waves developing along the body surface were measured in the experiments. It was found that the disturbances in the boundary layer were dominated by the second mode instability. Significant super harmonic components of the second modes were observed after the second mode became dominant. Compared with similar hypersonic flow over a sharp cone, the second mode instability of the blunt cone appeared in much further downstream locations. This indicates a stabilization of the boundary layer by slight nose bluntness. Stability experiments of hypersonic flows over sharp or blunt cones have also been carried out by other researchers. Demetriades [4, 5] had done extensive stability experiments on hypersonic boundary layers over axisymmetric

* Graduate Student, Mechanical and Aerospace Engineering Department. jxlei@ucla.edu
† Professor, Mechanical and Aerospace Engineering Department. Associate Fellow, AIAA. xiaolin@seas.ucla.edu

cones. Recently, Maslov and his colleagues [6, 7] reported their stability experiments on supersonic and hypersonic flows over sharp or blunt cones.

The normal-mode linear stability characteristics of the boundary-layer flow over the same blunt cone as Stetson *et al.*'s experiments have been studied by a number of researchers [8-11]. Malik *et al.* [8] computed the neutral stability curve and compared the growth rates obtained by LST with the experimental results. The steady base flow solution was computed by using the parabolized Navier-Stokes equations. They found that the nose bluntness stabilizes the boundary layer. The growth rates predicted by the LST were compared with Stetson *et al.*'s experimental results at the surface location of $s = 175$ nose radii (0.667 m). The linear stability analyses predicted slightly lower frequency for the dominant second mode, but much higher amplification rates than the experimental results. Rosenboom et al. [12] did further study on the effect of nose bluntness on the linear stability of hypersonic flow over Stetson's blunt cone. In their studies, the cone geometry and freestream conditions were adapted to the Stetson's experiments. Three cases of blunt cones of different nose radii, which cover both ``small'' and ``large'' bluntness, were considered. The purpose was to investigate, by linear stability analysis, the transition reversal phenomenon observed in experiments at ``large'' bluntness [13, 14]. By a linear stability analysis, Rosenboom et al. confirmed a monotonic downstream movement of the second mode critical Reynolds number as nose radius increases. However, their linear stability analysis still cannot explain the transition reversal phenomena observed in experiments at ``large'' bluntness.

Zhong et al. [15-17] have conducted numerical simulation of the stability and receptivity of Stetson's Mach 8 flow over blunt cones. In [16], the numerical results for the steady base flow were compared with the experimental results of Stetson et al [2], and with the numerical results of Esfahanian[18]. In addition, a normal-mode linear stability analysis was used to identify the main components of boundary-layer disturbances generated by forcing freestream fast acoustic waves. It was found that neither the first mode nor the second mode instability waves are excited directly by freestream fast acoustic waves in the early region along the cone surface, although the Mack modes can be unstable there. Instead, the second mode is excited downstream of the second-mode Branch I neutral stability point. The delay of the second-mode excitation is a result of the fact that the hypersonic boundary-layer receptivity is governed by a two-step resonant interaction process: 1) resonant interactions between the forcing waves and a stable boundary-layer wave mode I near the leading edge region, and 2) resonant interactions between the induced stable mode I and the unstable second Mack mode downstream.

In [17], Zhong conducted a numerical study on the effects of nose bluntness on the receptivity to free-stream acoustic waves for hypersonic flow by comparing the results of three nose radii. The flow conditions duplicated the experiments of Stetson et al. [2] and investigated the effects of nose bluntness on receptivity. Three nose radii were chosen to be the same as those used in Rosenboom et al.'s stability analysis. They are 3.81 mm (Case A), 17.78mm (Case B), and 42.67mm (Case C). The first nose radius belonged to category of ``small'' nose bluntness, while the second and third cases fell into the region of ``large'' bluntness. By using the numerical simulation, the initial receptivity process was computed accurately. The effects of bow shock interaction with forcing waves, the effects of the entropy layer and non-parallel boundary layer are also taken into account in the numerical simulation. A total of 15 frequencies are computed in the receptivity simulation for each case. It is found that, in those three test cases, the basic

receptivity mechanism of hypersonic flow over the blunt cone with different nose radii is essentially the same. Specifically, the receptivity is a result of the resonant interactions between forcing waves and boundary-layer wave modes near the nose region, and the resonant interactions between different boundary-layer wave modes downstream. As the nose radius increases from ``small'' to ``large'', the results in [2] showed no reversal in the location of instability wave induced by the receptivity process. In other words, the location of initial excitation of the second instability mode always moved downstream as the nose bluntness was increased.

Therefore, currently, the small bluntness effects of transition delay can be explained by the reduction of local Reynolds numbers. However, the mechanisms of transition reversal are not clear for the larger bluntness effects. The possible explanation for the experimental observation of transition reversal can be the instability of entropy layers, the surface roughness effects, wind tunnel noise in conventional noise tunnel, etc. So far, LST and computational studies have been done only on the test cases of Stetson's Mach 8 experiments [2]. All previous calculations have found no instability reversal at very large nose radii. On the other hand, Stetson's Mach 8 test model was not long enough to observe transition in his experiments. In other words, transition reversal phenomenon was not actually observed experimentally in Stetson's Mach 8 test cases. It is worthwhile to study, by both numerical simulation and LST, the mechanisms of transition reversal on the actual experimental conditions which have showed transition reversal.

Though the delay of transition by slight nose blunting has been found by many experiments since 1950s, the transition reversal at large nose bluntness has only been reported by a few researchers. Stetson et al. [1, 19] were the first ones to report concrete results on transition reversal. The only other reversal results were reported by Softley [20] on a Mach 10 flow over blunt cones with a half angle of 5 degree.

The most extensive experimental results on transition reversal are those reported by Stetson especially the case of Mach 5.5 flow over sharp and blunt cones [1] and similar experiments by Softley [20]. Transition data obtained in these test models is re-plotted in *Figure 1*(left), which shows the transitional Reynolds numbers vs. free stream Reynolds numbers based on nose radii. This figure is created by using Stetson's experimental results tabulated in Table 2 of [1]. The figure shows a clear transition reversal as Re_n increases, with the Re_n of 2×10^5 as the dividing line between "large" and "small" nose radii. These results are very similar to the transition reversal results of Softley collected from the case of between freestream Mach 10 to 12 flows over blunt cones as shown in *Figure 1*(right).

So far, there have not been LST and DNS studies on the Stetson's Mach 5.5 cases and Softley's cases, which are among the very few experimental test cases actually showing transition reversal. We have done some preliminary calculations on the Stetson's case [21, 22]. It will be valuable if these experiments can be systematically re-analyzed by modern DNS and linear stability techniques to study the effects on transition by nose bluntness. The experimental results on the parametric effects on transition can be compared with the computations. Therefore, the objectives is to continue our previous studies to conduct the LST and DNS studies of the cases of Stetson's Mach 5.5 on the nose bluntness effects. In this paper, we present both the DNS and LST results of three test cases of different nose radii: 0.156, 0.5 and 1.5 in. We will simulate

hypersonic flows over blunt cones corresponding to the flow conditions of this set of experiment, where transition reversal was observed. We will use a fifth-order shock-fitting code to compute the Navier-Stokes equations for such flows [23]. The code has been used to study the steady and unsteady hypersonic flow over a 7 degree blunt cone of Stetson's 1984 experiments [16, 17]. The use of high-order shock fitting schemes makes it possible to obtain highly steady and unsteady accurate solution of hypersonic flow over the cones with entropy layer effects. The steady mean flows then will be used as the base flows for the LST analysis. The unstable second mode growth rate will be calculated using a multi-domain spectral collocation method, which also have been tested in various study cases and proven to be reliable. Following that, the range of unstable second mode frequency can be identified for each case, which will be used as the forcing frequency for the unsteady numerical simulations. Also, the second mode N factor will be computed once the growth rates are obtained. It will be used to compare the predicted transition location based on LST to the transition location reported in the experiment. Lastly, through the LST analysis, we can take a closer look into the how the second mode is excited, which is hard to do using the numerical simulation.

2. GOVERNING EQUATIONS AND NUMERICAL METHOD

Steady Base Flow

The steady base flow solution is the solution of flow filed with no disturbance introduced. It was done by solving the full Navier-Stokes equations. The advantage of solving the full Navier-Stokes equations is that it contain least amount of approximation such that, if implement correctly, it can resolve the flow field with very high accuracy. The governing equations are the unsteady three-dimensional Navier-Stokes equations written in the following conservative form:

$$\frac{\partial U^*}{\partial t^*} + \frac{\partial F_j^*}{\partial x_j^*} + \frac{\partial F_{vj}^*}{\partial x_j^*} = 0 \qquad \textbf{(1)}$$

where $U^* = (\rho^*, \rho^* u_1^*, \rho^* u_2^*, \rho^* u_3^*, e^*)$, and superscript "*" represents dimensional variables. The Cartesian coordinates are denoted by (x_1^*, x_2^*, x_3^*) in tensor notation. In the current simulation of axisymmetric flow over blunt cones, x^* is along the centerline of the cone toward the downstream direction. The origin of coordinate is located at the center of spherical nose.

For numerical computation, is more convenient to deal with the dimensionless quantities. The flow velocities are nondimensionlized by the free-stream velocity U_∞^*, similarly, the length, density, pressure, temperature and time are nondimensionlized by $r_n^*, \rho_\infty^*, p_\infty^*, T_\infty^*$ and r_n^*/U_∞^*, etc. The dimensionless variables are presented by dropping the superscript "*".

A fifth-order shock-fitting method of Zhong [28] is used to compute the flow field bounded by the bow shock and cone surface. The flow variables behind the shock are determined by Rakine-Hugoniot relations across the shock and a characteristic compatibility equation behind the shock. Since the performance of the linear stability analysis is very sensitive to the base flow solution, the base flow must be very accurate in order to obtain the correct result for linear stability analysis. The shock-fitting scheme had been proven accurate and reliable by comparing with both experimental results from Esfahanian & Herbert [12] and the experimental results of Stetson *et al* [6].

Linear Stability Theory

The linear stability theory (LST) is used to study the instability of hypersonic flow over blunt cones in this paper. Based on the LST, the disturbances are limited to small amplitude and do not interact with each other unless at the synchronization point. The normal mode of disturbances is assumed to have the following form:

$$q' = \hat{q}(y_n) e^{i(-\omega t + \alpha s)} \tag{2}$$

where q' can be any flow variable such as velocity, temperature, density and pressure. And $\hat{q}$ is the eigenfunction representing the complex amplitude of the disturbance. In the spatial stability theory, ω, the dimensionless frequency of a normal disturbance mode , must be a real number. $\alpha = \alpha_r + \alpha_i$ is the stream-wise wave number, which is a complex number. The imaginary part of wave number is the spatial growth rate of a specific disturbance mode. When α_i turns negative, the disturbance becomes unstable. The real part of wave number α_r represents the spatial wave number. An important quantity that can be extracted from α_r is the phase velocity, which is defined as

$$a = \frac{\omega}{\alpha_r} = 10^{-6} \frac{FR}{\alpha_r} \tag{3}$$

In the above equation, a is the dimensionless phase velocity normalized by the free-stream velocity. F is dimensionless frequency such that

$$F = 10^6 \frac{\omega^* \upsilon_\infty^*}{U_\infty^{*2}} \tag{4}$$

R is local Reynolds number based on the length scale of boundary layer thickness. And s^* is the curvilinear coordinate along the cone surface measuring from the nose.

$$R = \frac{\rho_\infty^* U_\infty^* L^*}{\mu_\infty^*}, \tag{5}$$

$$L^* = \sqrt{\frac{\mu_\infty^* s^*}{\rho_\infty^* U_\infty^*}} \tag{6}$$

One of the most common applications of LST analysis in predicting the laminar-turbulent is to calculate the N factors based on a semi-empirical method called e^N method. From the theory, the transition will occur when the increment in amplitude of the disturbances reach certain critical level. The ratio of the amplitude of disturbances with fixed frequency can be calculated as they travel downstream. Since the growth rate is not a constant, the amplitude ratio between two locations can be expressed as an integral:

$$e^N = \frac{A}{A_0} = \exp \int_{s_0^*}^{s^*} \frac{1}{A} \frac{dA}{ds} ds^* \tag{7}$$

Or, just for the N factor,

$$N = \int_{s_0^*}^{s^*} -\alpha_i^* \, ds^* \tag{8}$$

In Eq.(8), s_0^* corresponds to the location that the disturbance just becomes neutrally stable. By computing this integral, we know how much the amplitude for a specific disturbance changes as it moves downstream. On the other hand, the N factor leading to transition is determined from the experimental measurement. The N factor is not unique for all the cases. It does depend on the flow conditions, object geometry and other unknown parameters. Even in one single case, the N factor differs when different unstable modes are considered. Here, the different unstable modes refer to the first mode and second mode introduced by Mack. In general, the N factor for first mode is smaller than the one for second mode. For high Mach number flow (Ma>4), the second mode is most unstable. Therefore, the N factor calculated in this paper is sorely for the second mode instability waves.

3. TEST CASES and FLOW CONDITIONS

The flow conditions for the test case studied in this paper are the same as those in Stetson's experiments on air flow over a blunt cone in a Mach 5.5 freestream [1]. For the case of zero angle of attack, Stetson tested ten blunt cones of different nose radii ranging from 1/32 in to 1.5 in. A range of different freestream unit Reynolds numbers were used to test these cones, from $1.6\times10^6/ft$ to $18\times10^6/ft$. In this paper, only three cases of different nose radii and a constant unit Reynolds number are used in the numerical simulation. The nose radii of the three cases are:

Case 1: $r_n = 1.5in = 38.1mm$

Case 2: $r_n = 0.5in = 12.7mm$

Case 3: $r_n = 0.15625in = 3.969mm$

The actual flow conditions used for the numerical simulation, which are identical in all three cases, are:

- $M_\infty = 5.468$
- $P_\infty^* = 7756.56\,Pa$, $T_\infty^* = 174.46K$
- Wall temperature: $T_w = 296K$
- $\gamma = 1.4$, $\mathrm{Pr} = 0.72$, $R^* = 286.94Nm/kgK$
- Freestream unit Reynolds number: $\mathrm{Re}_\infty^* = 18.95\times10^6 m^{-1}$
- Blunt cone half angle: $\theta = 8^o$, the freestream flow has a zero angle of attack
- Parameters in Sutherland's viscosity law: $T_r^* = 288K$, $T_s^* = 110.33K$, $\mu_r^* = 0.17894\times10^{-4}\,kg/ms$

where p_∞^* and T_∞^* are freestream pressure and temperature respectively. The body surface boundary condition is a non-slip condition for velocity and isothermal wall condition for temperature. In this particular study, both the steady base flow and unsteady flows are restricted to zero angle of attack.

4. SIMULATION of STEADY/UNSTEADY FLOW

As mentioned in previous section, the base flows are computed using fifth-order shock-fitting scheme with multiple zone approach. Each zone has a grid size of 240 by 240 by 4 in x, y and z direction respectively. The simulations are carried up to 0.8m, 1.8m and 3.2 m along the cone surfaces for the case with nose radius of 0.156, 0.5 and 1.5 inch. The detail of the results had been discussed in Zhong's paper [21]. In the current paper, only comparison of the contour of local unit Reynolds number for the three cases is showed (*Figure 2*) to demonstrate the nose bluntness effect on delay of the transition.

The unsteady simulations were performed by imposing a wall blowing and suction perturbation at the surface of the cone. The surface blowing and suction is applied by specifying perturbations to the wall normal velocities in the following form,

$$v_{n,wall}(x,t) = \varepsilon \sin\left[\alpha_w (x - x_0)\right] \sum_{n=1}^{N} A_n \cos(\omega_n t + \phi_n) \qquad (x_0 < x < x_1) \qquad \textbf{(9)}$$

In order to make comparisons with the linear stability results, the disturbance amplitude was set to small enough to insure the growth of instabilities was within the linear regime. For the current simulation, the amplitude ε is set to 10^{-5}. For the case of 1.5 inch nose radius cone, 15 frequencies ranged from 17517.0 Hz to 262754.3 Hz were imposed. The blowing and suction was placed at 0.1 m away from the nose tip along the cone surface. The unsteady waves are generated downstream of the blowing and suction slot. *Figure 3* plots the contours of the real part of the disturbance waves in temperature and tangential velocity. The disturbance wave patterns can be clearly observed on these contours.

After the LST analysis was conducted, it was found that the set of frequencies for the case of 1.5 inch cone is too low to capture the instability waves. The actual range will be presented in the next section. However, comparison was able to make to substantiate the LST results in the stable region. In *Figure 4*, the wave numbers versus the cone surface distance calculated by both the unsteady numerical simulation and LST analysis for a specific frequency of 262754 Hz are showed for case 1. A well agreement is established between the DNS and LST results on the wave numbers in this comparison. Also, the wave speeds obtained from both DNS and LST match up very well in *Figure 5*. In addition, this figure clearly indicates that the excited mode comes from the fast acoustic wave with a non-dimensional wave speed about 1+1/M. It will be showed later than this mode which is stable at the current location will become the unstable second mode at a higher frequency. Detail on mode analysis will be discussed in next section again. Here, the comparisons are to show that the LST results can be verified by the unsteady numerical simulation.

In order to provide a more realistic disturbance environment for natural transition, another type of forcing was also set up for the unsteady simulation. In this unsteady simulation, the free-stream fast acoustic waves were added in front of the shock, so the disturbances were allowed to interact with the shock structure. The disadvantage of this simulation is it requires a large amount of computational time. Some preliminary results have been obtained. However, the analysis is still undergoing, so the results will not be presented in the current paper.

5. LINEAR STABILITY RESULTS

From the base flow data obtained by the shock-fitting scheme, the unstable second modes for all three cases with different nose radii are successfully identified. The second mode dimensional growth rates versus the curvilinear distance along the surface of the blunt cone are presented in *Figure 6* for the three cases with different nose radii. Some common characteristics are observed in these cases. The disturbance with higher frequency turns unstable at location closer to the nose tip. As the frequency of the disturbance decrease, the peak value of second mode growth rate become higher. Among the three cases, the location where the second mode instability wave first appears consistently moves toward further downstream as the nose bluntness increases. Also, the range of unstable mode frequency keeps shifting to the lower end as the nose becomes blunter. The shift of frequency range can be explained but the increase of boundary layer thickness by blunting the nose, which causes the wave lengths of unstable modes become larger.

Figure 8 shows the wave speed and growth rate of the case with the nose radius of 0.156 inch for the disturbance frequency equals to 656886Hz only. In the non-dimensional growth rate plot, the negative value indicate unstable wave. By correlating with the wave speed figure, it is showed that the unstable mode is actually mode F, a discrete mode stems from the fast acoustic wave. The normalized fast acoustic wave have a value equals to 1+1/M, where M is the Mach number at the edge. Similarly, the slow acoustic wave is defined with speed of 1-1/M. In the same figure, the mode S is also plotted to demonstrate the phenomena called synchronization. Synchronization is a resonance between two normal modes of identical frequency when they reach the same wave speed. In this specific frequency, the synchronization occurs at about 0.42 m. The mode S becomes unstable Second mode is commonly seen in other studies [16], while this is the first case showing that the mode F becomes unstable second mode. The wave speed and growth rate figures for a fixed frequency share many similarities with those at a fixed location with various frequencies. In *Figure 9*, the wave speeds and growth rates versus the non-dimensional angular frequency at a fixed location s=0.42 m are plotted. These plots are very similar to the previous ones. Especially around the synchronization point, a clearly energy exchange is observed between mode S and mode F for both fixed-frequency and fixed-location plots.

As the second mode growth rates are calculated, the N factors can be found by integrating the growth rates along the cone surface. In *Figure 7*, the second mode N factors for all three cases of different nose bluntness are presented. By comparing the current LST results to the experimental transition data reported by Stetson [1], discrepancies in the transition locations are found. For the two cases with nose radius of 12.7mm and 38.1mm, the experiment showed transitions occurred at 0.421m and 0.243m, while no second mode instability were found at these locations according to the LST analysis. Traditionally, the N factor for transition has a value between 10 and 15. If taking N factor equals to 10 as the transition prediction criteria, the case1 and case2 predict that the transitions occur at 1.9 m and 0.7 m respectively. For case1, the N factor calculations do not even show a substantially large growth up to 3.2 m from the nose tip. In Table 1, some of the experiment and LST results are summarized.

Table 1 comparison of LST and experimental results

Nose radius	Free stream Re based on nose radius	Experimental transition location	N factor Based on Transition data	Instability onset location based on LST
3.969 mm	75213	0.406 m	2.3	0.3 m
12.7 mm	240665	0.421 m	N/A	0.8 m
38.1 mm	721995	0.243 m	N/A	1.9 m

Lastly, the eigenfunctions or mode shapes of mode F and mode S at location before, around and after the synchronization point are presented to observe the influence of mode interaction and to get a better understanding of the generation of second mode. In *Figure 10*, the eigenfunction of mode F in pressure, temperature and u velocity disturbance with frequency of 656886 Hz are plotted for the case 3. From *Figure 8*, it is known that the synchronization location of this frequency is at s=0.42m. So, the before, around and after locations of synchronization are chosen to be 0.3m, 0.42m and 0.6 m respectively. By comparing the shapes of eigenfunctions, it is found that the temperature disturbance profiles of mode F change drastically before and after synchronization while other two disturbances remain in similar shapes. The eigenfunctions of Mode S with the same frequency are showed in *Figure 11*. An interesting phenomenon is observed for the temperature perturbation of mode S, that is the peak of this mode quickly amplifies as the mode S moves downstream. At s=0.58 the peak reach a value above 8000, which make the assumption of linear perturbation no longer valid. If that is the case, the non-linear effect must be taking into account.

6. CONCLUSIONS/REMARKS

The Stetson's experiments with a free-stream Mach 5.5 conducted in 1967 are investigated using LST analysis and verified by unsteady numerical simulations. The ranges of second mode instability frequency for cones with nose radius of 0.156, 0.5 and 1.5 inch are identified. The growth rate and N factors are computed for each case. For the case in which the transition reversal was observed, the N factors based upon the second mode do not match with the experimental measurements. The second mode transition N factor for the case of 0.156 inch nose radius cone is too weak to be the dominant mechanism causing the transition. This implies that transition reversals are not caused by the second mode instabilities. Since the experiments were performed in a quiet noisy environment, there is likelihood that the reversal is cause by some uncontrollable noise with the amplitude large enough that the LST analysis and small perturbation numerical simulation are longer reliable. The Next step to unveil the secret of transition reversal is to conduct a numerical simulation with non-linear disturbance amplitudes.

Acknowledgments

This work was sponsored by AFOSR/NASA National Center of Hypersonic Research in Laminar-Turbulent transition and by the Air Force Office of Scientific research, USAF, under A Grants No. \FA9550-04-1-0029 and FA9550-07-1-0414, monitored by Dr. John Schmisseur. It was also supported by AFOSR STTR phase I Grant monitored by Jonathan Poggie at AFRL, at

Dayton, Ohio and John Schmisseur at AFOSR. The views and conclusions contained herein are those of the authors and should not be interpreted as necessarily representing the official policies or endorsements either expressed or implied, of the Air Force Office of Scientific Research or U.S. Government

References:

1. Stetson, K.F., Rushton, G. H., *Shock Tunnel Investigation of Boundary-Layer Transition at M = 5.5.* AIAA JOURNAL, 1967. **5**(5): p. 899-906.
2. Stetson, K.F., Thompson, E. R., Donaldson, J. C., and Siler, L. G., *Laminar Boundary Layer Stability Experiments on a Cone at Mach 8, Part 2: Blunt Cone.* 1984. AIAA paper 84-0006.
3. Stetson, K.F.a.K., R., *On the Breakdown of a Hypersonic Laminar Boundary Layer.* 1993. AIAA Paper 93-0896.
4. Demetriades, A., *Hypersonic Viscous Flow Over A Slander Cone. Part III: Laminar Instability and Transition.* AIAA paper 74-535, 1974.
5. Demetriades, A., *Laminar Boundary Layer Stability Measurements at Mach 7 Including Wall Temperature Effects.* AFOSR-TR-77-1311, 1977.
6. Maslov, A.A., Shiplyuk, A. N., Sidorenko, A., and Arnal, D., *Leading-edge Receptivity of a HypersonicBoundary Layer on a Flat Plate.* Journal of Fluid Mechanics, 2001. **426**: p. 73-94.
7. Maslov, A.A., Mironov, S. G., Shiplyuuk, A. A., Sidorenko, A. A., Buntin, D. A., and Aniskin, V. M., *Hypersonic Flow Stability Experiments.* 2002. AIAA 2002-0153.
8. Malik, M.R., Spall, R. E., and Chang, C. L., *Effect of Nose Bluntness on Boundary Layer Stability and Transition.* 1990. AIAA Paper 90-0112.
9. Herbert, T.a.E., V., *Stability of Hypersonic Flow over a Blunt Body.* AGARD CP, 1993. **514**: p. 28.
10. Kufner, E., Dallmann, U., and Stilla, J., *Instability of Hypersonic Flow Past Blunt Cones - Effects of Mean Flow Variations.* 1993. AIAA paper 93-2983.
11. Kufner, E., and Dallmann, U. *Entropy and Boundary Layer Instabilityof Hypersonic Cone Flows - Effects of Mean Flow Variations*. in *IUTAM Symposium on Laminar-Turbulent Transition*. 1994. Sendai/Japan: Springer-Verlag, Berlin.
12. Rosenboom, I., Hein, S., and Dallmann, U., *Influence of Nose Bluntness on Boundary-Layer Instabilities in Hypersonic Cone Flows* AIAA Paper 99-3591, 1999.
13. Potter, J.L., and Whitfield, J. D. *Boundary-Layer Transition under Hypersonic Conditions*. in *Recent Developments in Boundary Layer Research, Part III*. 1965.
14. Ericsson, L.E., *Effects of Nose Bluntness and Cone Angle on Slender Vehicle Transition.* AIAA Paper 87-1415, 1987.
15. Zhong, X., *Numerical Simulation and Experimental Comparison of Hypersonic Boundary Layer Instability over a Blunt Cone.* AIAA paper 2004-2244, 2004.
16. Zhong, X., and Ma, Y., *Boundary-layer receptivity of Mach 7.99 Flow over a blunt cone to free-stream acoustic waves.* Journal of Fluid Mechanics, 2005. **556**: p. 55-103.
17. Zhong, X., *Effect of Nose Bluntness on Hypersonic Boundary Layer Receptivity over a Blunt Cone.* AIAA paper 2005-5022, 2005.
18. Esfahanian, V., *Computation and stability analysis of laminar flow over a blunt cone in hypersonic flow*. 1991, The Ohio State University.
19. Stetson, K.F., *Nosetip Bluntness Effects on Cone Frustum Boundary Layer Transition in Hypersonic Flow.* AIAA paper 1983-1763, 1983.
20. Softley, E.J., *Transition of the Hypersonic Boundary Layer on a Cone: Part II - Experiments at Mach 10 and More on Blunt Cone Transition*, in *GE Space Science Lab, R68SD14*. 1968.
21. Zhong, X., *Numerical Simulation of Hypersonic Boundary Layer Receptivity and Stability on Blunt Circular Cones.* AIAA paper 2009-0940, 2009: p. 1-20.
22. Lei, J., and Zhong, X., *Linear Stability study of Hypersonic Boundary Layer Transition on Blunt Circular Cones* AIAA Paper 2009-0939, 2009.
23. Zhong, X., *High-Order Finite-Difference Schemes for Numerical Simulation of Hypersonic Boundary-Layer Transition.* Journal of Computational Physics, 1998. **144**: p. 662-709.
24. Zhong, X., *Leading-Edge Receptivity to Free Stream Disturbance Waves for Hypersonic Flow over a Parabola.* Journal of Fluid Mechanics, 2001. **441**: p. 315-367.

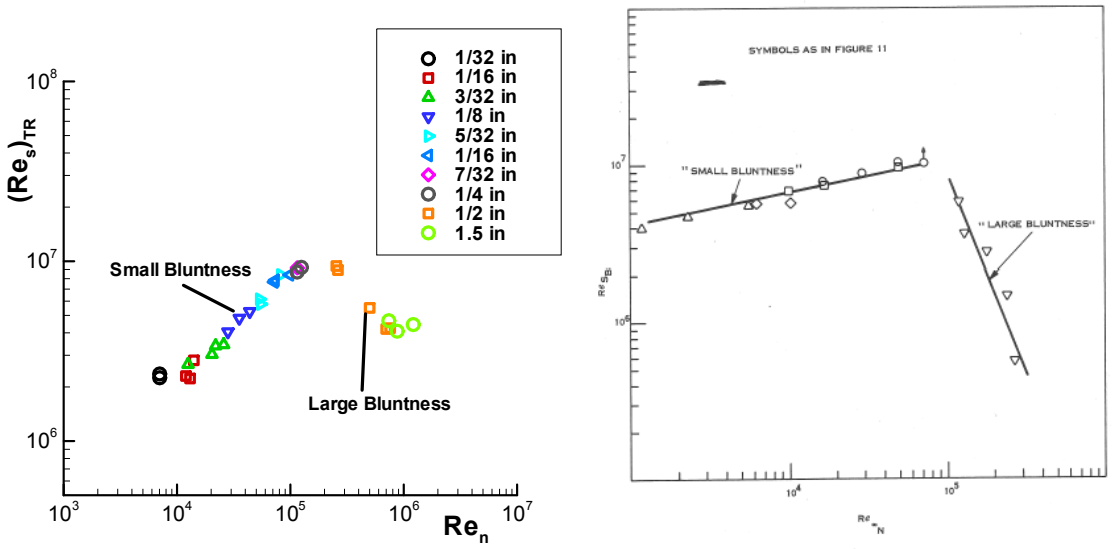

Figure 1. Transition Reynolds number vs. Reynolds number based on nose radius reported by Stetson(left) replot fromTable2 in [1] and Softley(right) in [20]

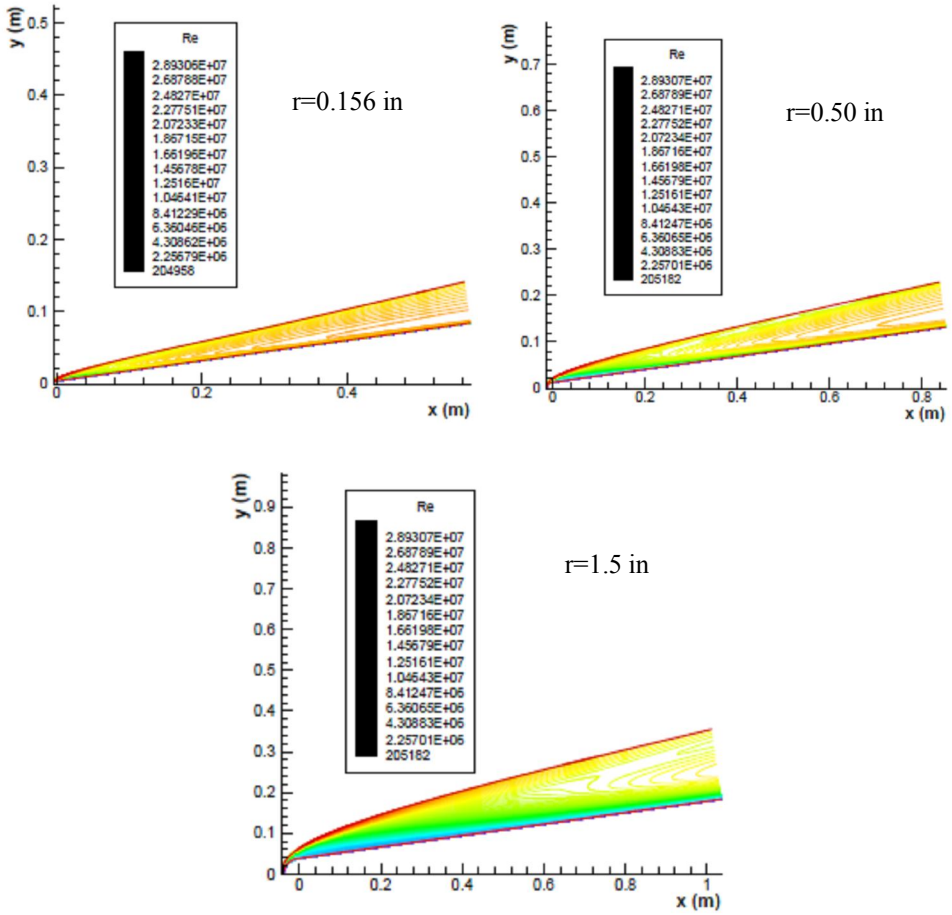

Figure 2. Contours of the local unit Reynolds numbers for the base flows with different nose radii

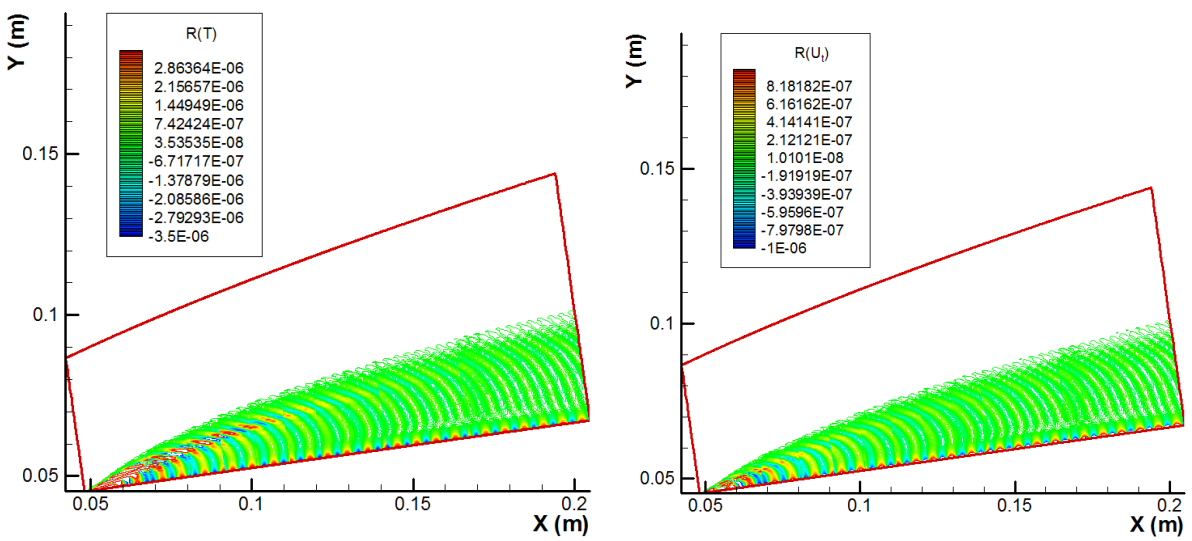

Figure 3. Contours of temperature (Left) and velocity (Right) disturbances of unsteady simulation with frequency of 262754 Hz for the case r=1.5 in.

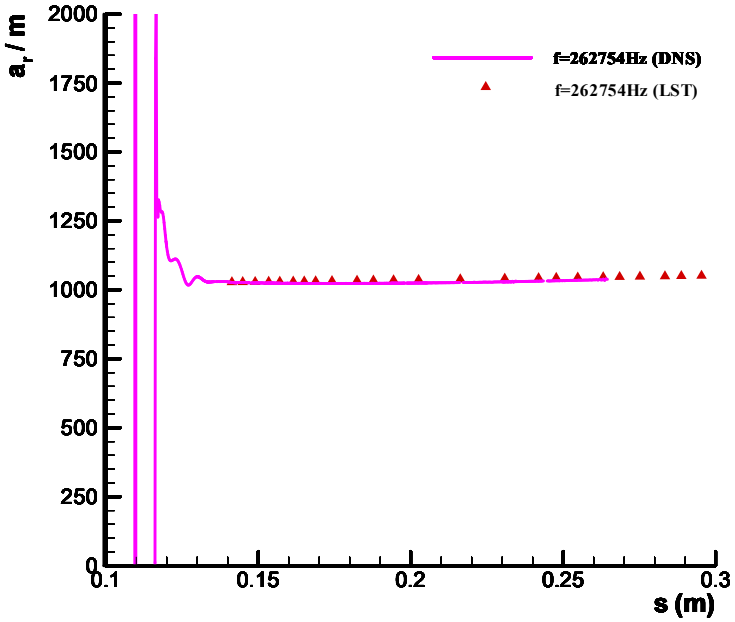

Figure 4. Comparison of wave numbers from DNS and LST with the disturbance frequency of 262754 Hz for the case r=1.5 in.

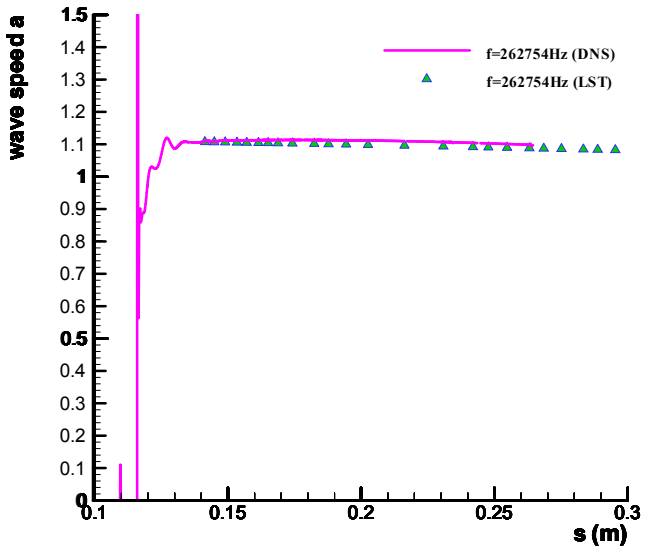

Figure 5. Comparison of wave speeds from DNS and LST with the disturbance frequency of 262754 Hz for the case r=1.5 in

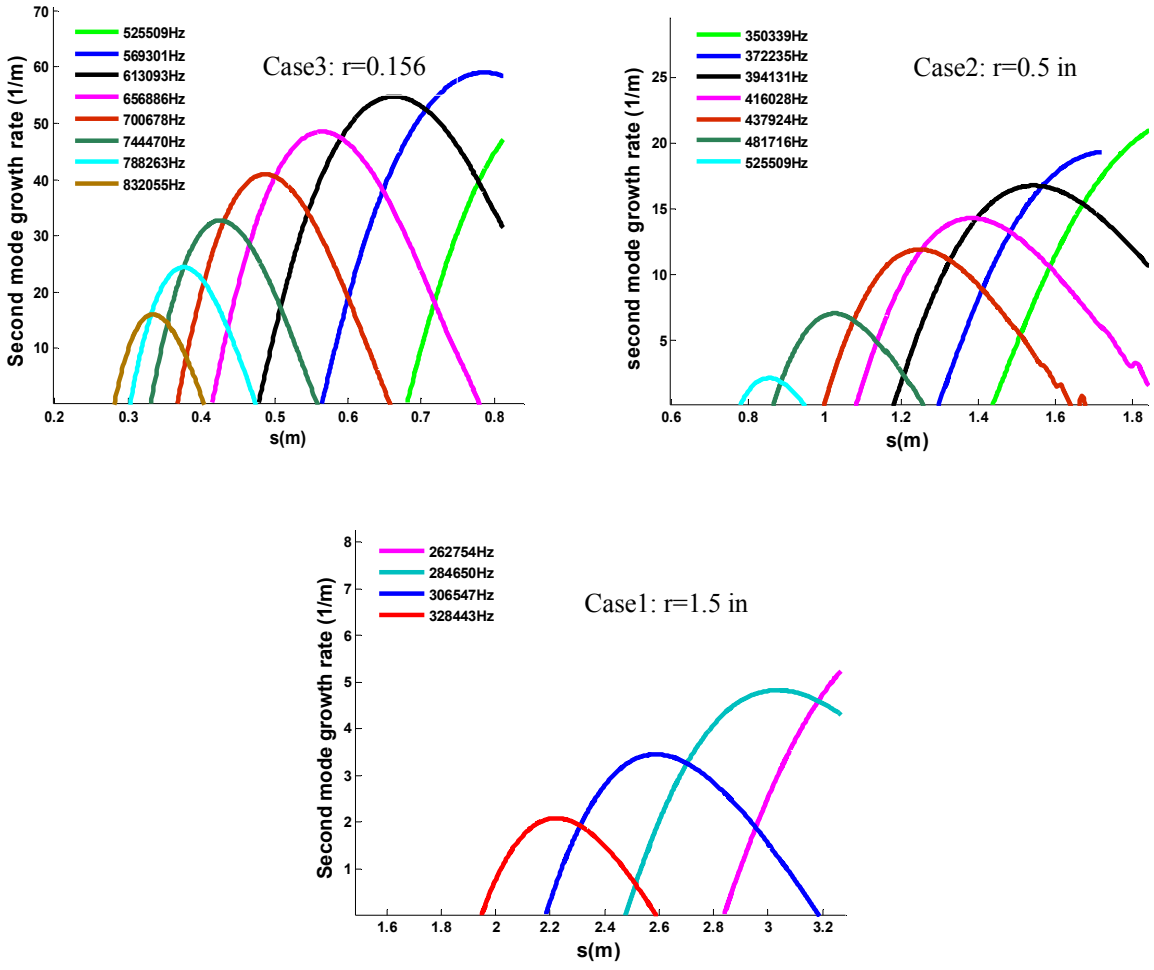

Figure 6. Second mode dimensional growth rates for the three cases with different nose radii

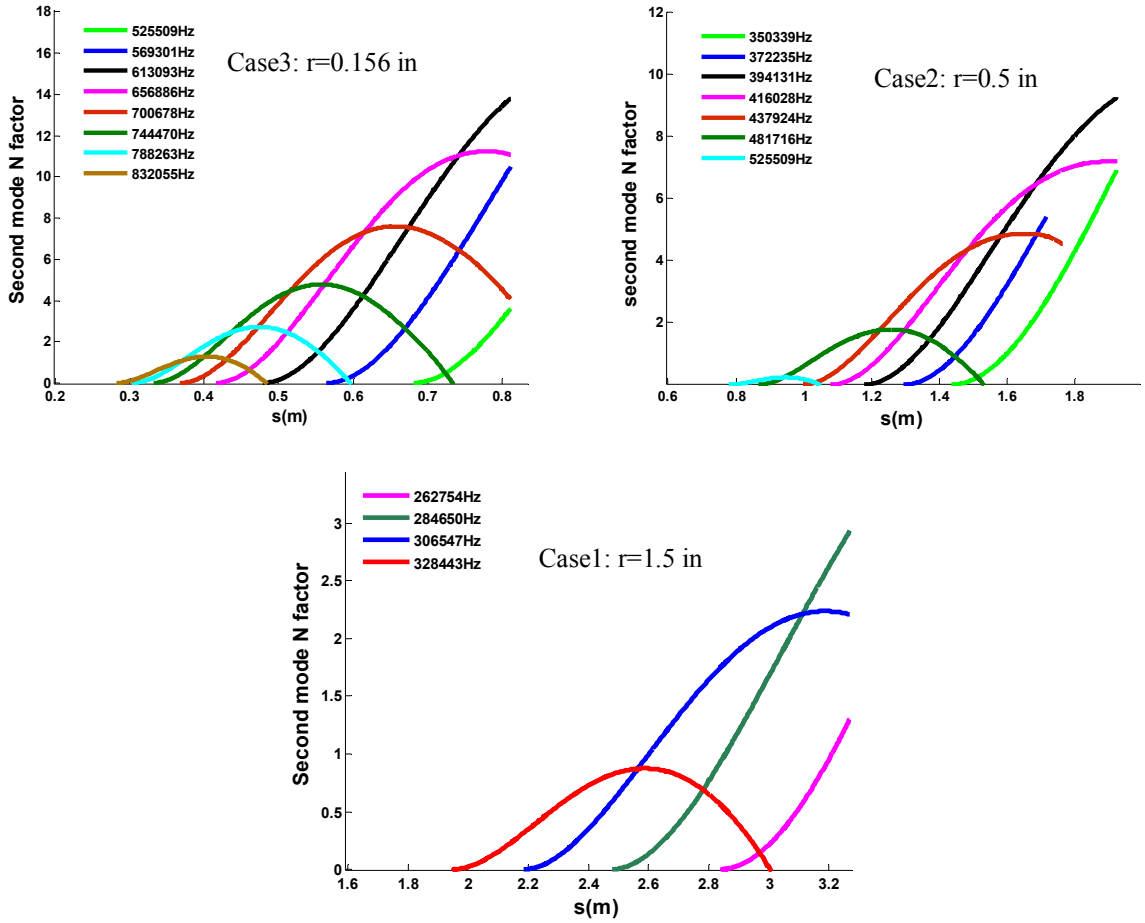

Figure 7. Second mode N factors for the three cases with different nose radii

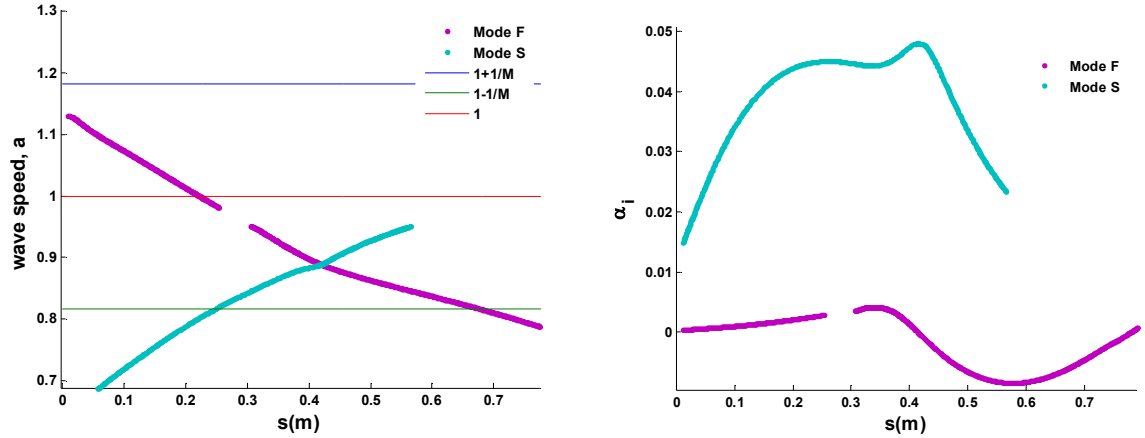

Figure 8. LST second mode wave speed (L) and non-dimensional growth rates (R) with the disturbance frequency of 656886 Hz for the case r=0.156 in

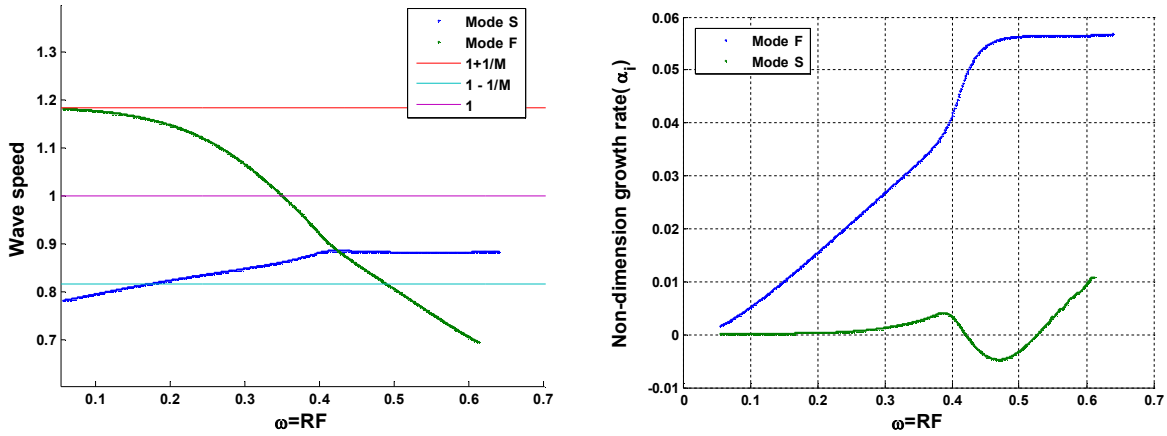

Figure 9. LST second mode wave speed (L) and non-dimensional growth rates (R) at location S=0.41 m for the case r=0.156 in

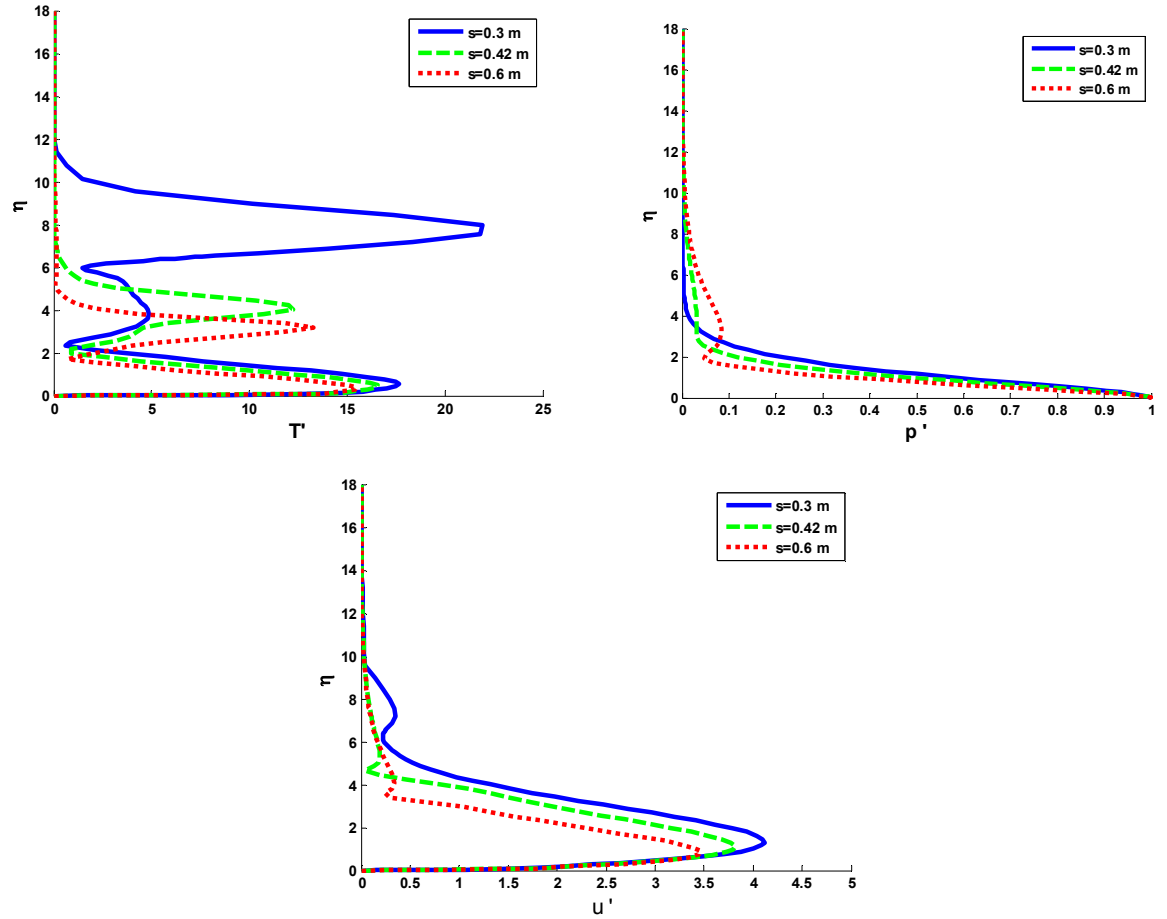

Figure 10. Eigenfunctions of temperature, pressure and u velocity of Mode F at different locations with the disturbance frequency of 656886 Hz for the case r=0.156 in

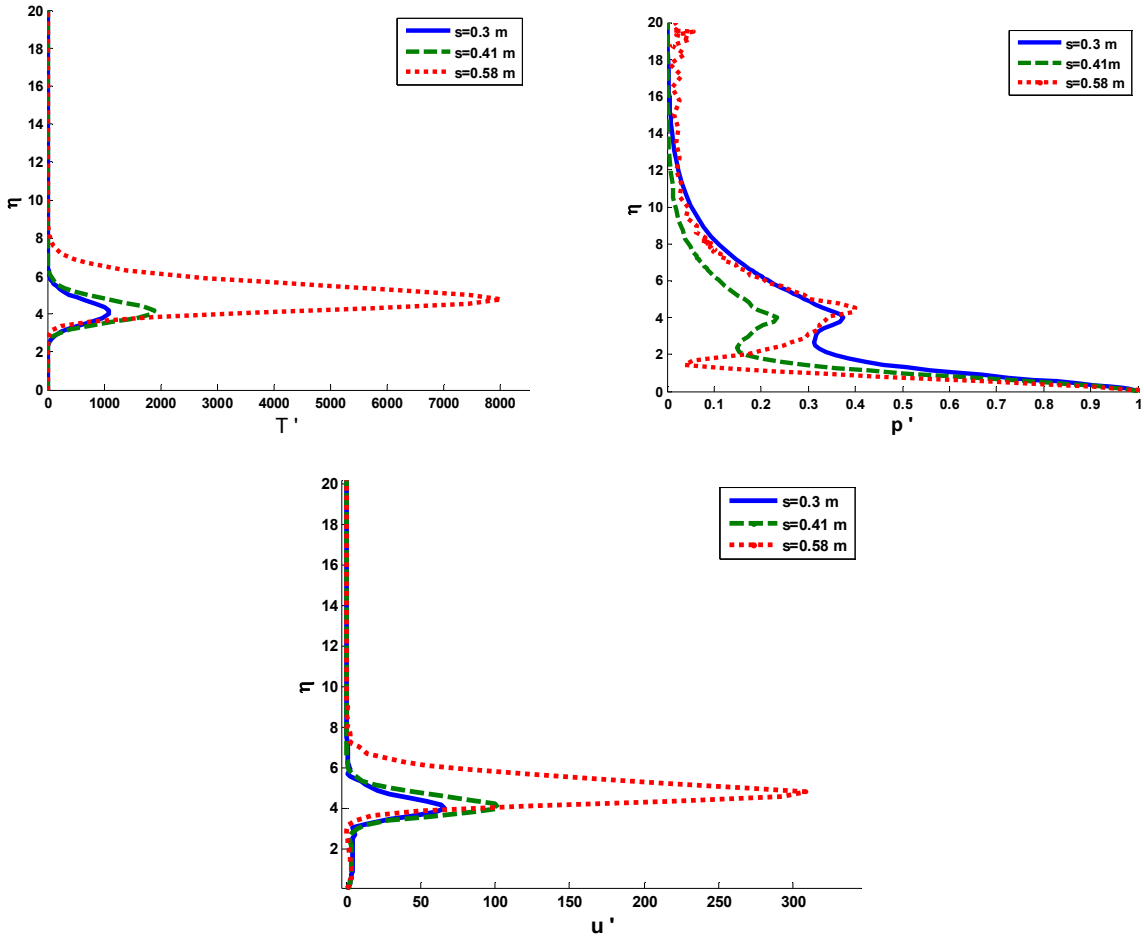

Figure 11. Eigenfunctions of temperature, pressure and u velocity of Mode S at different locations with the disturbance frequency of 656886 Hz for the case r=0.156 in